Introduction to $K_S K_S$ Physics at GlueX

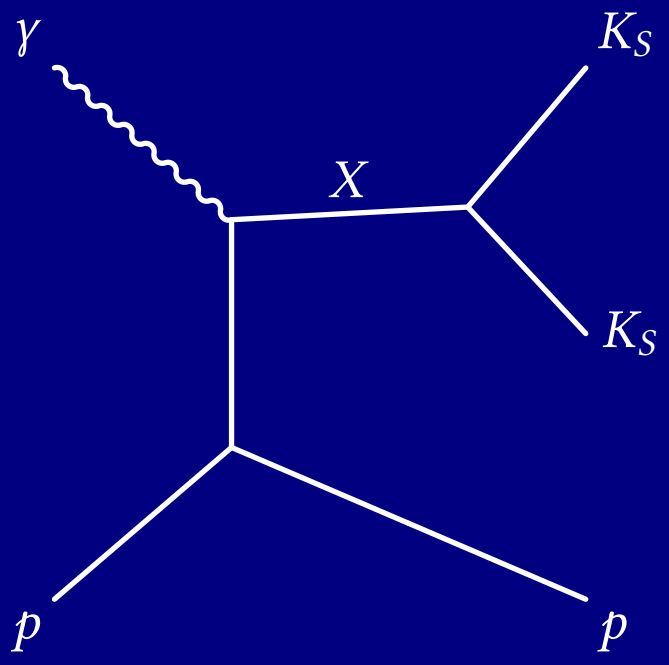

Nathaniel Dene Hoffman

Carnegie Mellon University

Table of Contents

Chapter 1

Introduction

1.1 A Brief History of Particle Physics

Since the days of the ancient Greeks, scientists and philosophers alike have been interested in the fundamental question concerning the composition of the universe. While the Greeks maintained that the world was composed of four indivisible elemental substances (fire, earth, air, and water) [1], this was at best a guess by the early philosophers, who had no mechanism with which to test their theory. Ironically, these philosophers struggled with a question to which us modern physicists still have no answer: Are the building blocks of the natural world fundamental (indivisible) [2]?

In 1808, John Dalton published a manuscript which described what is now called the "law of multiple proportions" after compiling several observations on chemical reactions which occur with specific proportions of their reactants. He anglicized the Greek *atomos*, meaning "not able to be cut", into the word we are familiar with—"atom" [3]. Towards the end of the century, J. J. Thomson demonstrated that cathode rays could be deflected by an electrostatic field, an observation which could not be explained by the prevailing theory that the rays were some form of light [4]. Instead, he proposed that these rays were made up of charged particles he called "corpuscles" (later renamed to the familiar "electrons") [5]. Around the same time (between 1906 and 1913), Ernest Rutherford, Hans Geiger, and Ernest Marsden conducted experiments in which they scattered alpha particles through a thin metal foil, and, through an analysis of the scattering angles, concluded that a positively charged nucleus must exist at the center of atoms, surrounded by electrons [6].

Over the next several decades, the nucleus was further divided into protons and neutrons[1] [7, 8]. In 1964, Murray Gell-Mann and George Zweig proposed a theory that protons and neutrons (and all other baryons and mesons) were

[1]For the discovery of the electron and neutron, Thomson and James Chadwick won Nobel Prizes in Physics in 1906 and 1935, respectively. Rutherford won the 1908 Nobel Prize in Chemistry for his research in radiation. However, I want to emphasize that while I mention the "big names" here, there are many who contributed in relative obscurity.

in fact composed of smaller particles Gell-Mann called "quarks"[2] [9]. These particles, along with the electron-like family of leptons (including neutrinos), the gauge bosons, and the Higgs boson, discovered in 2012 [10], comprise the Standard Model, a mathematical model which describes all the known forces and matter of the universe, with the notable exceptions (at time of writing) of gravity, dark matter, dark energy, and neutrino masses.

This thesis begins at a time when physicists are working hard to find gaps in this model, mostly by probing higher and higher ranges of energy. The experimental work being done at GlueX, however, resides in a lower energy regime, which we usually describe as "medium energy physics". As I will elucidate later in this manuscript, the strong force is non-perturbative in this regime, making direct calculations through the Standard Model all but impossible. However, since the advent of Lattice Quantum Chromodynamics (LQCD) in 1974 [11], physicists have been able to make approximate predictions via computer simulations of the theory.

1.2 Thesis Overview

Herein, I will focus on a particular portion of the Standard Model that dictates the strong interaction, viz. interactions between quarks and gluons, the mediating gauge boson of the strong force. Beginning with a discussion of the theory and history of K_S (K-short) pair production in prior experiments, I will give a brief overview of the GlueX experiment. I will then outline some of the theoretical underpinnings and implications of glueballs to persuade the reader on the importance of this production channel in the larger scheme of GlueX.

Next, I will describe my own analysis, beginning with the the impetus of this study, a search for Σ^+ baryons using a different recombination of the final state in this channel. This will lead to a first-order peek at the many resonances which decay to K_S pairs, and I will delineate the layers of data selection which I have carried out to produce a clean sample of events.

I will then discuss the process of partial-wave analysis (PWA), modeling resonances, and selecting a waveset for my data. I will conclude with the results from fits of these models to the data, the implications of such fits, and the next steps which I or another future particle physicist might take in order to illuminate another corner of the light mesonic spectrum.

1.3 Motivation

While this will be discussed in detail later, I believe it is important to emphasize the motivation for such a study of photoproduction of K_SK_S. While the majority of GlueX research concerns the study of hybrid mesons (mesons with forbidden quantum numbers), such mesons cannot be found in this channel. Given a bound state of two spin-$\frac{1}{2}$ quarks

[2] Upon reading the section of Finnegan's Wake which Gell-Mann cites as inspiration behind the name, I found (somewhat surprisingly) that the word "quark" was originally intended to rhyme with "mark", "ark", "lark", "bark", and so on, viz. [kwɑːrk] rather than the more common [kwɔːrk]!

with relative angular momentum L, total spin S and total angular momentum J (the eigenvalue of $\hat{J}^2 = \hat{L}^2 \oplus \hat{S}^2$), we can define the parity operator $\hat{P}$ by its effect on the wave function of the system,

$$\hat{P}\left|\vec{r}\right\rangle = \eta\left|\vec{r}\right\rangle \tag{1.1}$$

where η can be determined by noting that states of angular momentum are generally proportional to a spherical harmonic in their angular distribution ($|r, \theta, \varphi; LM\rangle \sim Y_L^M(\theta, \varphi)$) and

$$\hat{P}Y_L^M(\theta, \varphi) = Y_L^M(\pi - \theta, \pi + \varphi) = (-1)^L Y_L^M(\theta, \varphi) \tag{1.2}$$

so $\eta = (-1)^L$. The Dirac equation can be used to show that the intrinsic parity of quarks and antiquarks, when multiplied, yields a factor of -1, so

$$\hat{P}\,|q\bar{q}; JLMS\rangle = -(-1)^L \tag{1.3}$$

Similarly, the operator $\hat{C}$ representing C-parity will also introduce a factor of $(-1)^L$ because exchanging charges of a (neutral[3]) quark-antiquark system is akin to reversing their positions under parity. If $|S\rangle$ is antisymmetric under C-parity, we should get an additional factor of -1, which is the case for the $S = 0$ singlet. With the aformentioned -1 due to the intrinsic parity of the quarks and antiquarks, we find

$$\hat{C}\,|q\bar{q}; JLMS\rangle = (-1)^{L+S} \tag{1.4}$$

Labeling states with the common J^{PC} notation, it can then be shown that states like 0^{--}, 0^{+-}, 1^{-+}, and 2^{+-} (among others) are not allowed states for $q\bar{q}$ mesons. As mentioned, the investigation of such states is the primary focus of the GlueX experiment. However, since the particle we are concerned with decays to two identical particles (K_S) which have a symmetric spatial wave function, and because this particle is a meson which follows Bose-Einstein statistics, the angular part of the total wave function must also be symmetric, i.e. $J =$ even integers. Furthermore, because parity is conserved in strong decays, and the state of two identical particles is symmetric under parity, the decaying meson must also have $P = +$. Finally, the strong interaction also conserves C-parity, and both kaons are neutral, so we can determine the J^{PC} quantum numbers of the resonance to be even^{++}. There should be no overlap here with the aformentioned hybrid mesons, but that does not mean the channel is not of interest to GlueX and the larger scientific community. Particularly, the lowest lying glueball states are predicted to not only share these quantum numbers, but exist in the middle of the mass range produced by GlueX energies[12]. To add to this, the spin-0 isospin-0 light flavorless mesons, denoted as f_0-mesons, are supernumerary, either due to mixing with a supposed light scalar glueball or by the presence of a light tetraquark (or both)[13].

However, it would be an understatement to say that the K_SK_S channel at GlueX is not the ideal place to be looking for either glueballs or tetraquarks. This is because, while we have excellent handles for reconstructing this

[3]For $\hat{C}$ to be Hermitian, and thus observable, acting it twice on a state should return the original state, so only eigenvalues of ± 1 are allowed. Therefore, only states which are overall charge neutral are eigenstates of $\hat{C}$.

channel, we have no ability to separate particles of different isospin with these data alone. This means that these f states will be indistinguishable from their isospin-1 partners, the a-mesons. At first glance, it might seem like a model of the masses of these particles would make it easy to separate them, even if they remained indistinguishable between resonant peaks, but with broad states like the $f_0(1370)$ and states which sit right on top of each other (like the $f_0(980)$ and $a_0(980)$, which also tend to interfere with each other), there is likely no unique mass model which can distinguish all of the possible states without relying on data from other channels.

The silver lining is that, due to the GlueX detector's state-of-the-art angular acceptance[14], we do stand a chance at separating spin-0 states from spin-2 states, and GlueX's polarized beam allows us to further understand the mechanisms at play by giving us some indication of the parity of the t-channel exchanged particle in the production interaction. We can also use this channel as a proving ground for more complex amplitude analysis involving a mass model, which could be extended to a coupled-channel analysis in the future.

1.4 Past Analyses

This is certainly not the first attempt to study K^0_S pair production. The earliest published experiment with a similar final state dates back to 1961, where researchers at CERN measured 54 events which ended in a final state which included two neutral kaons. Since only K^0_S eigenstates decayed inside the bubble chamber, several of these early experiments infered a final state of $K^0_S K^0_S$. For the majority of the 1960s and 1970s, research into this final state was dominated by pion beam production off a proton target, aside from a kaon beam experiment in 1977 (see Table 1.1). In the 1980s, several collaborations at DESY began studying electron-positron collisions, which imply an internal virtual photon fusion as the production mechanism. These experiments are an important counterpoint to those involving hadrons, since the glueball does not couple to photons, so any intermediate glueball production in these reactions should be heavily suppressed [15], although radial excitations should couple [16]. While the statistical power of these experiments was very small at first (relative to pion beam experiments), the L3 collaboration at LEP and Belle at KEKB provided larger data samples in the first two decades of the 2000s. Until this study, ITEP and BNL held the statistical lead in non-photon-fusion experiments, and we now present a dataset which is at least 2.5 times as large as either.

There has only been one prior experiment, published by the CLAS collaboration in 2018 [17], which used photoproduction as a means of accessing this channel. While the "golden channel" for glueball production remains radiative J/ψ decays to $K^0_S K^0_S \gamma$, since non-glueball intermediate processes converting charm quarks into strange quarks are suppressed, photoproduction could be effective at creating exotic hybrid states as well as glueballs due via the photon's hadronic component or Pomeron exchange [16]. Additionally, the CLAS experiment did not utilize the polarized photon beam capability at JLab, but the current analysis at GlueX does, and this access to linear photon

Channel	Collaboration	# Events	Year
$\pi^- p \to K^0_S K^0_S n$	CERN/PS	54	1961 [18]
$\pi^- p \to K^0_S K^0_S n$	BNL	19	1962 [19]
$\pi^- p \to K^0_S K^0_S n$	LRL	66	1962 [20]
$\pi^- p \to K^0_S K^0_S$ + neutrals	BNL	374	1966 [21]
$\pi^- p \to K^0_S K^0_S n$	LRL	426	1966 [22]
$\pi^- p \to K^0_S K^0_S n$	LRL	418	1967 [23]
$\pi^- p \to K^0_S K^0_S n$	CERN/PS	2559	1967 [24]
$\pi^- p \to K^0_S K^0_S n$	ANL/ZGS	1969	1968 [25] & 1969 [26]
$\pi^- p \to K^0_S K^0_S n$	CERN/PS	4820	1975 [27]
$\pi^- p \to K^0_S K^0_S n$	CERN/PS	6380	1976 [28]
$\pi^- p \to K^0_S K^0_S n$	ANL/ZGS	5096	1976 [29] & 1979 [30]
$K^- p \to K^0_S K^0_S$ + neutrals	CERN/PS	410	1977 [31]
$\pi^- p \to K^0_S K^0_S n$	BNL/MPS	1278	1980 [32]
$\pi^- p \to K^0_S K^0_S n$	BNL/MPS	29381	1982 [33]
$e^+e^- \to e^+e^- K^0_S K^0_S$	DESY/TASSO	100	1983 [34]
???	???	???	1986 (Bolonkin)
???	???	???	1986 (Baloshin)
$\pi^- p \to K^0_S K^0_S n$	BNL/MPSII	40494	1986 [35]
$e^+e^- \to e^+e^- K^0_S K^0_S$	DESY/PLUTO	21	1987 [36]
$K^- p \to K^0_S K^0_S \Lambda$	SLAC/LASS	441	1988 [37]
$e^+e^- \to e^+e^- K^0_S K^0_S$	DESY/CELLO	26	1988 [38]
$e^+e^- \to e^+e^- K^0_S K^0_S$	LEP/L3	62	1995 [39]
$pp \to pp K^0_S K^0_S$	Fermilab/E690	11182	1998 [40]
$\pi^- p \to K^0_S K^0_S$ + neutrals	ITEP	1000†	1999 [41]
$e^+e^- \to e^+e^- K^0_S K^0_S$	LEP/L3	802	2001 [15]
$\pi^- C \to K^0_S K^0_S + X$	ITEP	553	2003 [42]
$e^+e^- \to e^+e^- K^0_S K^0_S$	LEP/L3	870	2006 [43]
$\pi^- p \to K^0_S K^0_S n$	ITEP	40553	2006 [44]
$e^+e^- \to e^+e^- K^0_S K^0_S$	KEKB/Belle	900000‡	2013 [45]
$\gamma p \to K^0_S K^0_S p$	JLAB/CLAS	13500†	2018 [17]
$\gamma p \to K^0_S K^0_S p$	JLAB/GlueX	102331*	2025 (this analysis)

Table 1.1: Summary of all (known) past analyses involving production of K^0_S pairs. Note that this is possibly not exhaustive and does not include any studies which focus on decays of an intermediate state, i.e. $J/\psi \to \gamma K^0_S K^0_S$.
† - Estimated from plots.
‡ - Reported as three orders of magnitude larger than LEP's result from 2006, but exact count was difficult to estimate.
$*$ - Weighted number of events with $\chi^2_\nu < 3.0$.

polarization can inform us of the parity exchanged in production of such exotic states.

Chapter 2

Experimental Design and Data Selection

2.1 The GlueX Experiment

The GlueX Kinematic Fit

2.2 Data Selection for the $K_S K_S$ Channel

Fiducial Cuts

2.3 sPlot Weighting

At this stage in the analysis, we are running low on simple cuts which can improve the signal-to-background ratio in the dataset. We must now turn to more complex solutions of separating the signal from potential background seepage. The first method we will use to do this is sPlot[46][1], a weighting scheme which corrects the naïve probabilistic weights one might first think to construct (dubbed "inPlot").

We start by developing a model for the signal and background probability distribution functions (PDFs) for a "discriminating" variable. We could then weight each event by some normalized probability of it being in the signal distribution rather than the background:

$$w(x) = \frac{N_S f_S(x)}{N_S f_S(x) + N_B f_B(x)} \tag{2.1}$$

where x is the discriminating variable, $f_S(x)$ and $f_B(x)$ are the corresponding signal and background PDFs, and N_S and N_B are the total number of signal and background events, respectively.

However, as shown by Pivk and Le Diberder[46], we must be careful when using this procedure, as it will only correctly produce signal-isolated plots for "control" variables y which are directly correlated with x. For the time

[1] This is stylized as ${}_s\mathcal{P}lot$ in the original paper, but I find this tedious to type and to read.

being, let us assume that this is not the case, and that we wish to use the distribution of some variable which is uncorrelated with the variables we are plotting and analyzing[2]. Following the sPlot derivation, we find that, to plot uncorrelated control variables, we must weight our data according to the following scheme:

$$w(x) = \frac{V_{SS} f_S(x) + V_{SB} f_B(x)}{N_S f_S(x) + N_B f_B(x)}, \quad \text{where } V_{ij}^{-1} = \sum_x \frac{f_i(x) f_j(x)}{(N_S f_S(x) + N_B f_B(x))^2} \tag{2.2}$$

The V^{-1} matrix can also be understood as the covariance matrix between the free parameters N_S and N_B in the fit of the signal-background mixture, $V_{ij}^{-1} = -N \frac{\partial^2 \ln \mathcal{L}}{\partial N_i \partial N_j}$, although there is reason to believe that direct calculation by this method will lead to less accurate results than the manual calculation in Equation (2.2)[47].

Now that we have a method of assigning weights, we must pick the discriminating variable. Typically, these weighting methods work well on the classic "bump-on-a-background" distributions, but because the mass of the kaons is constrained in the kinematic fit, the fitted mass of each kaon is just a δ-function and combination of measured masses for each $\pi^+\pi^-$ pair will yield a Normal distribution with little to no apparent background (by construction), so we must be a bit more clever in determining a discriminating variable. By examining the BGGEN analysis done in [TODO: PREVIOUS SECTION], we can see that most likely sources of background arise when the intermediate kaons are missing from the reaction: $\gamma p \to 4\pi p$. This reaction shares the $K_S K_S$ final state exactly, so pairs of pions which look close enough to kaons will be almost indistinguishable in the data. However, they differ in one key way, namely that the K_S intermediate contains a strange quark while the $\pi^+\pi^-$ decay state does not, so such a decay must occur via the weak interaction, which is notably slower than the strong interaction which would produce pion pairs with no intermediate kaon. In other words, while the signal's rest-frame lifetime distribution should have an exponential slope near the K_S lifetime, the background would theoretically have nearly zero rest-frame lifetime for every event, or a much smaller exponential slope in practice.

Therefore, we will begin by generating both a signal and background dataset in Monte Carlo. We then interpret both datasets as if they were our desired channel by running them through the GlueX reconstruction and reaction filter, as well as all of our selections up to this point. We can then fit the rest-frame lifetime of each dataset to an exponential model,

$$f(t; \lambda) = \lambda \exp\{-\lambda t\} \tag{2.3}$$

where $\lambda \equiv 1/\tau$, the lifetime of the kaon in question. Since we have two independently decaying kaons, we should really form a joint distribution for both, where we will assume each kaon has the same average lifetime:

$$f(t_1, t_2; \lambda) = \lambda^2 \exp\{-\lambda t_1\} \exp\{-\lambda t_2\} \tag{2.4}$$

[2] We will later see that things are not quite so simple!

Both the signal and background distributions can be modeled in this way, giving us only two free parameters, λ_S and λ_B for the signal and background respectively, to fit.

Once we obtain nominal values for λ_S and λ_B from fits over the signal and background Monte Carlo, we can fix the exponential slopes to the fit values and perform a new fit to our real data with a mixture model:

$$\begin{aligned} g(t_1, t_2) &\equiv z f(t_1, t_2; \lambda)\Big|_{\lambda=\lambda_S} + (1-z) f(t_1, t_2; \lambda)\Big|_{\lambda=\lambda_B} \\ &= z\lambda_S^2 \exp\{-\lambda_S t_1\} \exp\{-\lambda_S t_2\} + (1-z)\lambda_B^2 \exp\{-\lambda_B t_1\} \exp\{-\lambda_B t_2\} \end{aligned} \tag{2.5}$$

In the fit to data, only the fraction of signal to background, z, is floating. From its fit value, we can determine values of N_S and N_B to use in **??** and complete the weighting procedure.

Non-Factorizing sPlot

Over the course of the previous discussion, it was assumed that the discriminating variable, t, was statistically independent from the control variable. To test whether this is indeed true, we need to first pick some control variables which we want to be able to use later. The set of control variables must include all variables we use as inputs to the partial-wave analysis in Chapter 3. This includes the invariant mass m of the $K_S^0 K_S^0$ system and the helicity angles θ and φ of the decay. To test for independence, we first split our dataset into M evenly-spaced quantiles in the control variable, which ensures each bin gets roughly the same number of events. Next, we calculate the likelihood of the null hypothesis, which assumes the variables are statistically independent, by fitting all datasets simultaneously with a shared λ parameter. We then calculate the likelihood of the alternative hypothesis, which assumes statistical dependence, by finding the joint likelihood of independent fits of λ over each quantile. The result of these fits can be formulated as a likelihood ratio,

$$\Lambda = -2 \ln \frac{\sup \mathcal{L}_{H_0}}{\sup \mathcal{L}_{H_1}} = -2 \ln \frac{\sup \prod_i^M \mathcal{L}_i(z_i, \lambda_S, \lambda_B)}{\sup \prod_i^M \mathcal{L}_i(z_i, \lambda_{S,i}, \lambda_{B,i})} \tag{2.6}$$

Λ is χ^2 distributed with $2M-2$ degrees of freedom (the difference between $M+2$ free parameters in the null hypothesis and $3M$ in the alternative hypothesis). Note that here, $\mathcal{L}_i$ denotes the likelihood evaluated over data in the ith quantile. The factor of 2 is required because $\ln \mathcal{L}(\theta_1, ..., \theta_i) \sim -\frac{1}{2}\chi_i^2$ asymptotically with sample size according to Wilks' theorem. We can obtain a p-value representing the likelihood of the null hypothesis being true by evaluating the p-value:

$$p = 1 - F_{\chi^2_{2M-2}}(\Lambda) = 1 - P\left(\frac{2M-2}{2}, \frac{\Lambda}{2}\right) \tag{2.7}$$

where $P(s,t)$ is the regularized gamma function. Following this procedure for the invariant mass of $K_S^0 K_S^{0\,3}$, the p-values for each number of quantiles and run period can be seen in the first four rows of Table 2.1 and in Figure 2.1, depicting the case with four quantiles. The calculated p-values tend to be very small, implying that we should reject the null hypothesis and accept that the discriminating (rest-frame lifetime) and control (invariant mass of $K_S^0 K_S^0$) variables are not statistically independent. This means we cannot use a traditional sPlot to weight our data. Fortunately, the process for obtaining the correct weights is straightforward, we simply allow for more than one signal and background component in the fit and sum over all signal components when we calculate the final weight values [47]. Since sPlot weights from different components can be added to each other to obtain a joint weight [46], Equation (2.2) can be extended to multiple signal and background components:

$$w_{\mathbb{S}}(x) = \frac{\sum_{i\in\mathbb{S}} \sum_j V_{ij} f_j(x)}{\sum_k N_k f_k(x)}, \quad \text{where } V_{ij}^{-1} = \sum_x \frac{f_i(x) f_j(x)}{\left(\sum_k N_k f_k(x)\right)^2} \tag{2.8}$$

and $\mathbb{S}$ is the set of signal components. We can further verify the need for non-factorizing sPlot by performing the factorization test described in Equations (2.6) and (2.7) to the signal and background Monte Carlo, with a slight modification to the number of free parameters, since we only need to fit either a signal or background component rather than a mixture:

$$p = 1 - P\left(\frac{M-1}{2}, \frac{\Lambda}{2}\right) \quad \text{where } \Lambda = -2\ln \frac{\sup \prod_i^M \mathcal{L}_i(\lambda)}{\sup \prod_i^M \mathcal{L}_i(\lambda_i)} \tag{2.9}$$

The results of these tests can also be found in the last eight rows of Table 2.1, and are visualized for four quantiles in Figure 2.2. There are enough significantly small p-values to justify the use of non-factorizing sPlot across both the signal and background components, meaning that we need at least two signal and two background components in the final sPlot weighting.

Application of Weights

The only thing left to do is determine how many signal and background components we should use in the weighting procedure. To this end, we now turn to the Monte Carlo simulations of the signal and 4π-background. By choosing a number of quantiles in invariant mass corresponding to the number of components, we can fit single exponential distributions to each quantile in the simulated signal and background. For instance, if we chose to use two signal components and three background components, we would divide the signal Monte Carlo into two quantiles and the background Monte Carlo into three, and fit each quantile to an exponential distribution to obtain a set of two λ_S and three λ_B values. The resulting λ_S and λ_B values could then be used as a starting point for a multi-component fit to the data. Alternatively, both the signal and background or just the signal could be fixed to the values from the fits

[3] No significant statistical dependence was found for the helicity angles.

		# quantiles		
		2	3	4
Data Type	Run Period	p	p	p
Data	Spring 2017	1.36×10^{-28}	1.92×10^{-27}	8.00×10^{-29}
	Spring 2018	3.38×10^{-08}	1.32×10^{-07}	6.09×10^{-09}
	Fall 2018	2.18×10^{-09}	5.44×10^{-15}	1.02×10^{-15}
	Spring 2020	9.86×10^{-171}	2.10×10^{-199}	1.08×10^{-198}
$K^0_S K^0_S$ MC	Spring 2017	$< 2.23 \times 10^{-308}$	$< 2.23 \times 10^{-308}$	$< 2.23 \times 10^{-308}$
	Spring 2018	$< 2.23 \times 10^{-308}$	$< 2.23 \times 10^{-308}$	$< 2.23 \times 10^{-308}$
	Fall 2018	$< 2.23 \times 10^{-308}$	$< 2.23 \times 10^{-308}$	$< 2.23 \times 10^{-308}$
	Spring 2020	$< 2.23 \times 10^{-308}$	$< 2.23 \times 10^{-308}$	$< 2.23 \times 10^{-308}$
4π MC	Spring 2017	9.53×10^{-01}	4.78×10^{-03}	5.62×10^{-02}
	Spring 2018	6.40×10^{-01}	9.78×10^{-01}	4.49×10^{-01}
	Fall 2018	1.54×10^{-05}	1.44×10^{-06}	6.46×10^{-07}
	Spring 2020	4.47×10^{-09}	2.36×10^{-08}	2.25×10^{-09}

Table 2.1: The probability of accepting the null hypothesis (that the rest-frame lifetime is statistically independent of the invariant mass of $K^0_S K^0_S$) for the tests described in Equation (2.6) for data and Equation (2.9) for Monte Carlo with the given number of quantiles. All values are calculated with a $\chi^2_\nu < 3.0$ selection on each type of data over each run period. Values listed as $< 2.23 \times 10^{-308}$ are nonzero but smaller than the smallest representable 64-bit floating point number

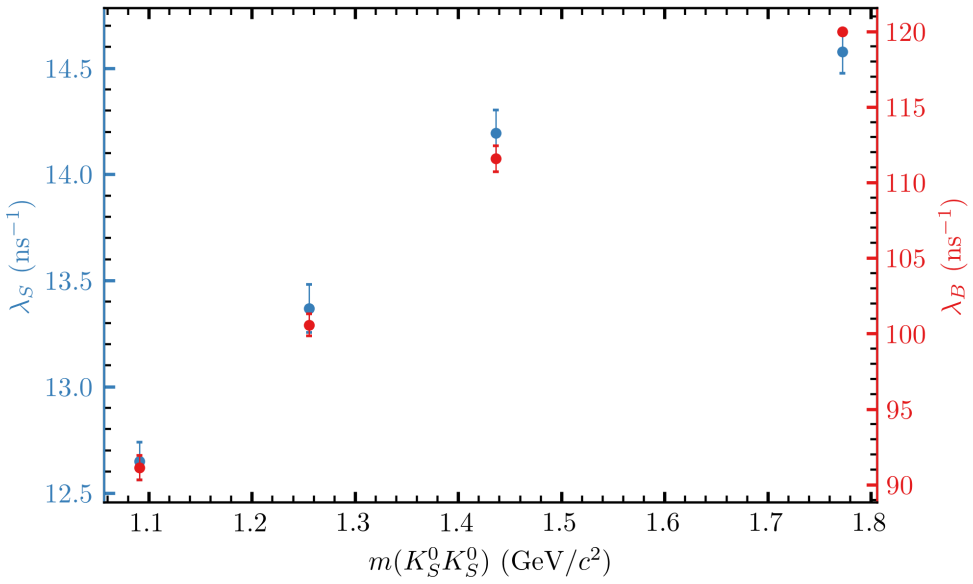

Figure 2.1: Exponential slopes from fits over four quantiles in $m(K^0_S K^0_S)$ (x-axis) to a mixture of signal (left y-axis) and background (right y-axis) components for the Spring 2020 run period. These fits show a definite statistical dependence between rest-frame lifetime and the invariant mass of $K^0_S K^0_S$, as described in Table 2.1. All values are calculated with a $\chi^2_\nu < 3.0$ selection on each type of data over each run period.

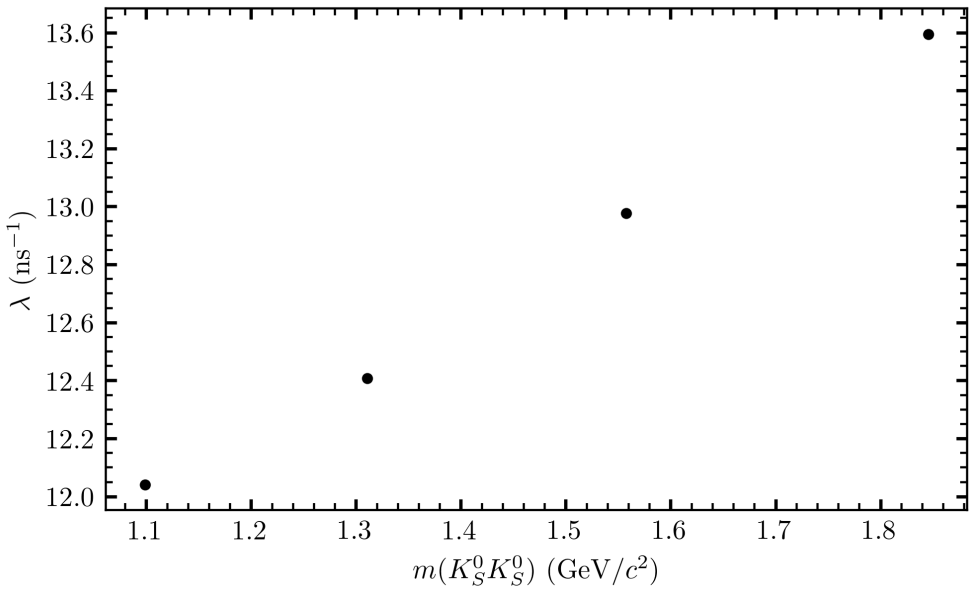

(a)

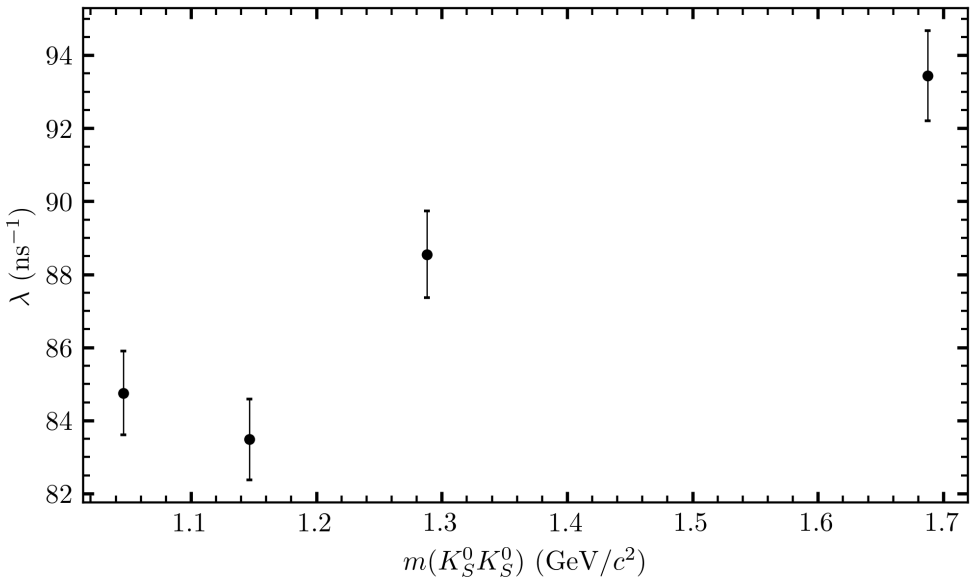

(b)

Figure 2.2: Exponential slopes from fits over four quantiles in $m(K_S^0K_S^0)$ (x-axis) of the signal (a) and background (b) Monte Carlo rest-frame lifetime distributions for the Spring 2020 run period. Both show a definite statistical dependence between rest-frame lifetime and the invariant mass of $K_S^0K_S^0$, as described in Table 2.1. All values are calculated with a $\chi_\nu^2 < 3.0$ selection on each type of data over each run period.

to simulations, and only the yields (or the yields and background λs) would be allowed to float in the fit to data. We will refer to the first case, where the fit parameters from Monte Carlo are free, as A, the case where the signal λs are fixed as B, and the case where all λs are fixed (and the only floating parameters are the yields of each component) as C. To select a model, we can use the relative Akaike Information Criterion (AIC) [48] and Bayesian Information Criterion (BIC) [49]:

$$r\text{AIC} \equiv \text{AIC} - \text{AIC}_{\text{min}} \quad \text{where AIC} \equiv 2k - 2\ln\mathcal{L} \tag{2.10}$$

$$r\text{BIC} \equiv \text{BIC} - \text{BIC}_{\text{min}} \quad \text{where BIC} \equiv k\ln N - 2\ln\mathcal{L} \tag{2.11}$$

$$\tag{2.12}$$

where k is the number of free parameters and N is the number of events in the dataset. The optimal model will minimize these criteria. In Table 2.1, all of the relative AIC and BIC values are shown. Excluding cases with only one signal or background component (restricting to models which have non-factorizing signal and background components), the minimizing values for most run periods tend to use two signal and two background components, and excluding the Spring 2020 dataset, they all use method B, where the signal components are fixed to values obtained from Monte Carlo while the background components are initialized at Monte Carlo values but allowed to float in the fit. For consistency, we will use method B with two signal and two background components, denoted $B(2,2)$, as our weighting method. See Figure 2.3. The selection of method B is also interesting as it could describe a case where another background which is not modeled in the background Monte Carlo is present and has a similar exponential slope. Since these slopes are free in the fit to the data, they may anticipate this unknown slope better than the fixed case (method C), and method B also explicitly assumes the Monte Carlo for true signal kaons is correct and fixes their component slopes (unlike method A).

	# Components		Spring 2017		Spring 2018		Fall 2018		Spring 2020	
Method	Signal	Background	*r*AIC	*r*BIC	*r*AIC	*r*BIC	*r*AIC	*r*BIC	*r*AIC	*r*BIC
A	1	1	0.000	0.000	0.000	0.000	0.000	0.000	51.876	8.573
	1	2	4.000	21.835	4.000	23.028	4.000	23.490	32.397	10.746
	1	3	8.000	43.668	8.002	46.059	8.005	46.985	36.827	36.827
	2	1	4.000	21.834	4.000	23.028	4.000	23.490	46.866	25.215
	2	2	8.000	43.669	8.004	46.061	8.000	46.980	0.000	0.000
	2	3	12.000	65.503	12.001	69.086	12.004	70.473	54.865	76.516
	3	1	8.000	43.669	8.000	46.057	8.000	46.980	31.906	31.906
	3	2	12.000	65.503	12.002	69.087	12.001	70.470	54.357	76.008
	3	3	16.001	87.338	16.000	92.114	16.003	93.962	0.897	44.200
B	1	1	51.318	42.400	46.523	37.008	78.990	69.245	435.265	381.136
	1	2	47.778	56.695	50.523	60.037	69.623	79.368	215.025	182.548
	1	3	51.126	77.878	54.524	83.066	72.976	102.210	222.971	212.146
	2	1	7.891	7.891	0.635	0.635	1.056	1.056	129.068	85.765
	2	2	11.891	29.725	4.635	23.663	5.057	24.547	52.986	31.334
	2	3	15.893	51.561	8.635	46.692	9.059	48.038	58.202	58.202
	3	1	2.496	11.413	3.770	13.284	2.411	12.156	75.783	43.306
	3	2	6.498	33.250	7.770	36.313	6.422	35.657	35.672	24.846
	3	3	10.496	55.082	11.770	59.341	10.411	59.135	40.264	51.090
C	1	1	215.228	197.394	639.813	620.785	695.587	676.098	2698.867	2633.913
	1	2	216.138	207.221	610.406	600.892	461.384	451.640	1822.845	1768.716
	1	3	169.934	169.934	624.358	624.358	352.522	352.522	1521.662	1478.359
	2	1	205.960	197.043	649.757	640.242	697.047	687.302	2695.194	2641.066
	2	2	206.778	206.778	619.947	619.947	453.115	453.115	1778.976	1735.673
	2	3	155.836	164.754	634.060	643.574	337.024	346.769	1455.471	1422.994
	3	1	209.102	209.102	645.091	645.091	695.880	695.880	2692.864	2649.561
	3	2	209.927	218.844	615.616	625.130	453.630	463.375	1781.688	1749.211
	3	3	159.336	177.171	629.602	648.630	338.314	357.803	1459.431	1437.780

Table 2.2: Relative AIC and BIC values for each fitting method (relative within each run period). The absolute minimum values in each column are underlined, and the minimums excluding models with only one signal or background component are boxed.

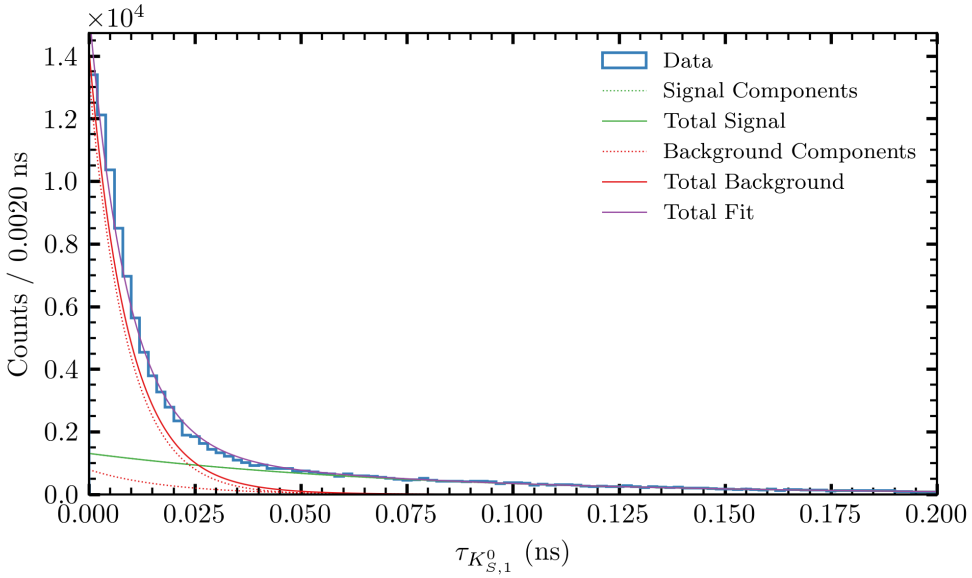

Figure 2.3: Fit of Equation (2.5) to data from the Spring 2020 run period using method $B(2,2)$. True kaon events are prominent in the tail of the distribution, whereas background events peak strongly near zero. All values are calculated with a $\chi^2_\nu < 3.0$ selection on each type of data over each run period. The second signal component tends to be very small but non-zero across all datasets.

Chapter 3

Partial-Wave Analysis

3.1 Amplitude Formalism

TODO: cite http://scipp.ucsc.edu/~haber/ph218/ExperimentersGuideToTheHelicityFormalism.pdf and S.U. Chung spin formalisms

Now we embark on the topic of amplitudes. We wish to describe the dynamics of our reaction in a way that allows us to extract quantum numbers like spin from our data. There are several difficulties in doing so: First, we are trying to determine the properties of many particles at once, and we know that many resonances in this channel overlap in mass space. This precludes the use of a simple Breit-Wigner description of most of these resonances, as overlapping Breit-Wigners do not preserve unitarityTODO: citation. Second, the GlueX experiment uses a linearly polarized photon beam, so it behooves us to use a formalism which can include this polarization. Finally, there are many resonances in this channel, and while we have the largest photoproduction dataset to date, we are still relatively data limited, which further complicates any dynamical description.

Single-Particle Helicity States

We begin by defining a set of observables which are independent of frames and rotations on those frames. This is known as the helicity formalism, where helicity resembles the spin projection along the axis of a particle's motion. First, we define a rotation $R(\alpha, \omega, \gamma)$ as a matrix whose action on a vector is a rotation about the Euler angles α, ω, and γ. For each rotation, we can define a unitary operator $U[R]$ which has the group property $U[R_2 R_1] = U[R_2]U[R_1]$ as it is an operator on the group $SO(3)$. Being an operator on $SO(3)$, we can also write it as

$$U[R(\alpha, \omega, \gamma)] = e^{-\imath\alpha J_z} e^{-\imath\omega J_y} e^{-\imath\gamma J_z} \tag{3.1}$$

We can then describe the matrix elements of this operator in the angular momentum eigenbasis $|jm\rangle$ (representing a spin-j particle where m is the projection of spin onto the $\hat{z}$-axis) with the Wigner D-matrix:

$$U[R(\alpha,\omega,\gamma)] \equiv \sum_{m'} |jm\rangle\, D^{j}_{m'm}(R(\alpha,\omega,\gamma)) \tag{3.2}$$

where

$$D^{j}_{m'm}(\alpha,\omega,\gamma) \equiv e^{-\imath m'\alpha} d^{j}_{m'm} e^{-\imath m\gamma} \tag{3.3}$$

and

$$d^{j}_{m'm}(\omega) = \left\langle jm' \middle| e^{-\imath\omega J_y} \middle| jm \right\rangle \tag{3.4}$$

We can further extend this eigenbasis to include linear momentum by introducing Lorentz boosts $L(\vec{\beta})$. We denote the operation of a boost along the $\hat{z}$-axis with velocity β as $L_z(\beta)$. A boost in any direction described by polar angles (θ,φ) can be achieved by rotating the $\hat{z}$-axis to align with the direction vector, boosting in the new $\hat{z}$-direction, and rotating back:

$$L(\vec{\beta}) = R(\varphi,\theta,0) L_z(\beta) R^{-1}(\varphi,\theta,0) \tag{3.5}$$

Together, the space of rotations and boosts defines the Lorentz group, where each arbitrary Lorentz transformation Λ has a unitary operator $U[\Lambda]$ with the group property $U[\Lambda_2\Lambda_1] = U[\Lambda_2]U[\Lambda_1]$, so in terms of operators, we can also write

$$U[L(\vec{p})] = U[R(\varphi,\theta,0)]U[L_z(p)]U^{-1}[R(\varphi,\theta,0)] \tag{3.6}$$

Finally, this allows us to define the "canonical" basis for a single particle as

$$U[L(\vec{p})]\,|jm\rangle \equiv \left|\vec{p}, jm\right\rangle \tag{3.7}$$

Unfortunately, the quantum number m is only valid in the rest frame of the state because the $\hat{z}$-axis of the rest frame is not equivalent to the $\hat{z}$-axis in any arbitrarily Lorentz-transformed frame. Therefore, we will define helicity λ as the projection of spin along the direction of motion and introduce new helicity states,

$$\left|\vec{p}, j\lambda\right\rangle = U[L(\vec{p})]U[R(\varphi,\theta,0)]\,|j\lambda\rangle = U[R(\varphi,\theta,0)]U[L_z(p)]\,|j\lambda\rangle \tag{3.8}$$

In this definition, we have two ways of obtaining the helicity frame: We can either rotate the state first such that the quantization axis is aligned with $\vec{p}$ and then boost in the $\hat{p}$-direction or we can first boost in the $\hat{z}$-direction and then rotate. In either equivalent case, λ is invariant under rotations as well as boosts parallel to $\vec{p}$. Finally, we can define these helicity states over a basis of canonical states:

$$\left|\vec{p}, j\lambda\right\rangle = \sum_m D^j_{m\lambda}(R(\varphi,\theta,0))\left|\vec{p}, jm\right\rangle \tag{3.9}$$

The single-particle states are normalized such that

$$\left\langle \vec{p}', j'\lambda' \middle| \vec{p}, j\lambda \right\rangle = \tilde{\delta}(\vec{p}' - \vec{p})\delta_{j'j}\delta_{\lambda'\lambda} \tag{3.10}$$
$$\text{with } \tilde{\delta}(\vec{p}' - \vec{p}) = (2\pi)^3(2E)\delta^{(3)}(\vec{p}' - \vec{p})$$

since the Lorentz-invariant phase space element is given by $\tilde{\mathrm{d}p} = \frac{\mathrm{d}^3\vec{p}}{(2\pi)^3(2E)}$. This gives the following representation of the identity:

$$\sum_{j\lambda} \int \left|\vec{p}, j\lambda\right\rangle \tilde{\mathrm{d}p} \left\langle \vec{p}, j\lambda\right| = I \tag{3.11}$$

Two-Particle Helicity States

Of course, we would like to extend these states to be able to talk about interactions and decays. For notation, I will use Ω to represent the polar angles θ and φ and $\varnothing$ to describe the specific value of 0 for both of these angles. Similarly, R_Ω and $R_\varnothing$ will represent the corresponding rotation operators (the second being a null rotation the direction of the $\hat{z}$-axis). R without subscript or angles will represent an arbitrary rotation whose angles are not important for the derivation.

Next, we can define a joint state of two particles with masses w_1 and w_2 (to avoid confusion with angular moments) and spins s_1 and s_2. In the center-of-momentum (COM) frame, these particles are back-to-back, and we can define the momentum of particle 1 as $\vec{p}$ with direction Ω and particle 2 as $-\vec{p}$. Then the joint canonical state, up to a normalization constant $\mathcal{N}$, is given by

$$|\Omega, s_1 m_1 s_2 m_2\rangle = \mathcal{N}\, U[L(\vec{p})]\,|s_1 m_1\rangle\, U[L(-\vec{p})]\,|s_2 m_2\rangle \tag{3.12}$$

Such a state can also be described with a total spin s and moment m_s:

$$|\Omega, s m_s\rangle = \sum_{m_1 m_2} (s_1 m_1 s_2 m_2 \mid s m_s)\,|\Omega, s_1 m_1 s_2 m_2\rangle \tag{3.13}$$

Here, $(s_1 m_1 s_2 m_2 \mid s m_s)$ is the Clebsch-Gordan coefficient describing the angular momentum coupling. Next, we can add additional angular momentum apart from the spin. For a system with angular momentum ℓ with moment m, we use the fact that $\langle\Omega|\ell m\rangle = Y^m_\ell(\Omega)$ (spherical harmonics) to define

$$|\ell m s m_s\rangle = \int \mathrm{d}\Omega\, Y^m_\ell(\Omega)\,|\Omega; s m_s\rangle \tag{3.14}$$

Next, the spin s and angular momentum ℓ can be coupled into the total angular momentum J with moment M:

$$|JM\ell m s m_s\rangle = \sum_{m\, m_s} (\ell m s m_s \mid JM)\,|\ell m s m_s\rangle \tag{3.15}$$

This coupled state is still in the canonical formalism, and we would like to use the helicity basis. Using Equation (3.8),

$$|\Omega, s_1\lambda_1 s_2\lambda_2\rangle = \mathcal{N}\, U[R_\Omega] \underbrace{\left(U[L_z(p)]\,|s_1\lambda_1\rangle\, U[L_{-z}(p)]\,|s_2, -\lambda_2\rangle\right)}_{|\varnothing, s_1\lambda_1 s_2\lambda_2\rangle} \tag{3.16}$$

To obtain states with a total angular momentum, we can integrate over the space of all rotations, weighted by Wigner D-matrices:

$$|JM s_1\lambda_1 s_2\lambda_2\rangle = \frac{N_J}{2\pi} \int \mathrm{d}R\, D^{J*}_{M\mu}(R) U[R]\,|\varnothing, s_1\lambda_1 s_2\lambda_2\rangle \tag{3.17}$$

This is, of course, incomplete, as we have not defined the normalization factor N_J or the coupling μ which relates helicities to total angular momentum. To do both, let us specify the rotation R as follows,

$$\begin{aligned}
|JM s_1\lambda_1 s_2\lambda_2\rangle &= \frac{N_J}{2\pi} \int \mathrm{d}R\, D^{J*}_{M\mu}(R) U[R(\varphi,\theta,\gamma)]\,|\varnothing, s_1\lambda_1 s_2\lambda_2\rangle \\
&= \frac{N_J}{2\pi} \int \mathrm{d}R\, D^{J*}_{M\mu}(R) U[R(\varphi,\theta,0)] U[R(0,0,\gamma)]\,|\varnothing, s_1\lambda_1 s_2\lambda_2\rangle \\
&= \frac{N_J}{2\pi} \int \mathrm{d}R\, D^{J*}_{M\mu}(R) e^{-\imath(\lambda_1-\lambda_2)\gamma} U[R(\varphi,\theta,0)]\,|\varnothing, s_1\lambda_1 s_2\lambda_2\rangle \\
&= \frac{N_J}{2\pi} \int \mathrm{d}\Omega\,\mathrm{d}\gamma\; e^{\imath M\varphi} d^{J*}_{M\mu} e^{\imath\mu\gamma} e^{-\imath(\lambda_1-\lambda_2)\gamma} U[R(\varphi,\theta,0)]\,|\varnothing, s_1\lambda_1 s_2\lambda_2\rangle \\
&= \frac{N_J}{2\pi} \int \mathrm{d}\Omega\,\mathrm{d}\gamma\; e^{\imath M\varphi} d^{J*}_{M\mu} e^{\imath(\mu-(\lambda_1-\lambda_2))\gamma}\,|\Omega, s_1\lambda_1 s_2\lambda_2\rangle \\
&= N_J \int \mathrm{d}\Omega\, D^{J*}_{M\lambda}(R_\Omega)\,|\Omega, s_1\lambda_1 s_2\lambda_2\rangle \\
&\text{with } \lambda = \lambda_1 - \lambda_2
\end{aligned} \tag{3.18}$$

It can be shown that the normalization $\mathcal{N} = \frac{1}{4\pi}\sqrt{\frac{p}{w}}$ where p is the relative momentum and w the effective mass of the two-particle system. The normalization of the standard two-particle states is given by

$$\left\langle \Omega', s_1'\lambda_1' s_2'\lambda_2' \middle| \Omega, s_1\lambda_1 s_2\lambda_2 \right\rangle = \delta^{(2)}(\Omega'-\Omega)\delta_{s_1' s_1}\delta_{\lambda_1'\lambda_1}\delta_{s_2' s_2}\delta_{\lambda_2'\lambda_2} \tag{3.19}$$

This follows immediately from Section 3.1. Next, to ensure that

$$\left\langle J'M' s_1'\lambda_1' s_2'\lambda_2' \middle| JM s_1\lambda_1 s_2\lambda_2 \right\rangle = \delta_{J'J}\delta M'M\delta_{s_1' s_1}\delta_{\lambda_1'\lambda_1}\delta_{s_2' s_2}\delta_{\lambda_2'\lambda_2} \tag{3.20}$$

we must have $N_J = \sqrt{\frac{2J+1}{4\pi}}$. Finally,

$$\left\langle \Omega, s_1' \lambda_1' s_2' \lambda_2' \middle| JM s_1 \lambda_1 s_2 \lambda_2 \right\rangle = N_J D^{J*}_{M\lambda}(R_\Omega) \delta_{s_1' s_1} \delta_{\lambda_1' \lambda_1} \delta_{s_2' s_2} \delta_{\lambda_2' \lambda_2} \tag{3.21}$$

Production Amplitudes

TODO: cite https://link.springer.com/article/10.1140/epjc/s10052-020-7930-x

3.2 Second attempt

Following https://onlinelibrary.wiley.com/doi/10.1155/2020/6674595

Figure 3.1: Absolute square of spherical harmonics for S- and D-waves integrated over φ.

Including Linear Polarization

3.3 The Z_ℓ^m Amplitude

3.4 The K-Matrix Parameterization

3.5 Waveset Selection

Chapter 4

Results and Systematic Studies

4.1 Mass-Independent Fits

4.2 Mass-Dependent Fits

4.3 Systematics

Chapter 5

Conclusion

Appendix A

Derivation of the Chew-Mandelstam Function

We begin with the dispersion integral[1]:

$$C(s) = C(s_{\text{thr}}) - \frac{s - s_{\text{thr}}}{\pi} \int_{s_{\text{thr}}}^{\infty} \mathrm{d}s' \, \frac{\rho(s')}{(s' - s)(s' - s_{\text{thr}})} \tag{A.1}$$

where $s_{\text{thr}} = (m_1 + m_2)^2$ and

$$\rho(s) = \sqrt{\left(1 - \frac{(m_1 + m_2)^2}{s}\right)\left(1 - \frac{(m_1 - m_2)^2}{s}\right)} \tag{A.2}$$

We first focus on just the integral part:

$$I(s) = \int_{s_{\text{thr}}}^{\infty} \mathrm{d}s' \, \frac{\rho(s')}{(s' - s)(s' - s_{\text{thr}})} \tag{A.3}$$

$$\lim_{\epsilon \to 0} \int_a^b \mathrm{d}x \, \frac{f(x)}{(x - x_0) + \imath\epsilon} = \fint_a^b \mathrm{d}x \, \frac{f(x)}{(x - x_0)} + \imath\pi f(x_0) \tag{A.4}$$

$$I(s) = \fint_{s_{\text{thr}}}^{\infty} \tag{A.5}$$

[1] see arXiv paper

Bibliography

[1] Aristotle. *Metaphysics*. Trans. by W. D. Ross. 1.4,985b10-15. type: classic. URL: http://classics.mit.edu/Aristotle/metaphysics.html.

[2] Aristotle. *Physics*. Trans. by R. P. Hardie and R. K. Gaye. 6.1-3,231a21-234b10. URL: http://classics.mit.edu/Aristotle/physics.html.

[3] John Dalton. *A New System of Chemical Philosophy*. In collab. with Smithsonian Libraries. Manchester: Printed by S. Russell for R. Bickerstaff, Strand, London, 1808. 248 pp. URL: http://archive.org/details/newsystemofchemi11dalt (visited on 06/12/2024).

[4] J. J. Thomson. "Cathode Rays". In: *Philosophical Magazine* 44 (1897), pp. 293–316.

[5] J. J. Thomson. *The Corpuscular Theory of Matter*. Scribner's Sons, New York, 1907.

[6] E. Rutherford. "LXXIX. The scattering of α and β particles by matter and the structure of the atom". In: *The London, Edinburgh, and Dublin Philosophical Magazine and Journal of Science* 21.125 (May 1, 1911). Publisher: Taylor & Francis _eprint: https://doi.org/10.1080/14786440508637080, pp. 669–688. ISSN: 1941-5982. DOI: 10.1080/14786440508637080. URL: https://doi.org/10.1080/14786440508637080 (visited on 06/12/2024).

[7] Orme Masson. "XXIV. The constitution of atoms". In: *The London, Edinburgh, and Dublin Philosophical Magazine and Journal of Science* 41.242 (Feb. 1, 1921). Publisher: Taylor & Francis _eprint: https://doi.org/10.1080/14786442108636219, pp. 281–285. ISSN: 1941-5982. DOI: 10.1080/14786442108636219. URL: https://doi.org/10.1080/14786442108636219 (visited on 06/12/2024).

[8] J. Chadwick. "Possible Existence of a Neutron". In: *Nature* 129.3252 (Feb. 1932). Publisher: Nature Publishing Group, pp. 312–312. ISSN: 1476-4687. DOI: 10.1038/129312a0. URL: https://www.nature.com/articles/129312a0 (visited on 06/12/2024).

[9] M. Gell-Mann. "A schematic model of baryons and mesons". In: *Physics Letters* 8.3 (Feb. 1, 1964), pp. 214–215. ISSN: 0031-9163. DOI: 10.1016/S0031-9163(64)92001-3. URL: https://www.sciencedirect.com/science/article/pii/S0031916364920013 (visited on 06/12/2024).

[10] G. Aad et al. “Observation of a new particle in the search for the Standard Model Higgs boson with the ATLAS detector at the LHC”. In: *Physics Letters B* 716.1 (Sept. 17, 2012), pp. 1–29. ISSN: 0370-2693. DOI: 10.1016/j.physletb.2012.08.020. URL: https://www.sciencedirect.com/science/article/pii/S037026931200857X (visited on 06/12/2024).

[11] Kenneth G. Wilson. “Confinement of quarks”. In: *Physical Review D* 10.8 (Oct. 15, 1974). Publisher: American Physical Society, pp. 2445–2459. DOI: 10.1103/PhysRevD.10.2445. URL: https://link.aps.org/doi/10.1103/PhysRevD.10.2445 (visited on 06/12/2024).

[12] Colin J. Morningstar and Mike Peardon. “Glueball spectrum from an anisotropic lattice study”. In: *Physical Review D* 60.3 (July 7, 1999), p. 034509. ISSN: 0556-2821, 1089-4918. DOI: 10.1103/PhysRevD.60.034509. URL: https://link.aps.org/doi/10.1103/PhysRevD.60.034509 (visited on 08/30/2024).

[13] Particle Data Group et al. “Review of Particle Physics”. In: *Progress of Theoretical and Experimental Physics* 2020.8 (Aug. 14, 2020), p. 083C01. ISSN: 2050-3911. DOI: 10.1093/ptep/ptaa104. URL: https://academic.oup.com/ptep/article/doi/10.1093/ptep/ptaa104/5891211 (visited on 08/30/2024).

[14] S. Adhikari et al. “The GlueX beamline and detector”. In: *Nuclear Instruments and Methods in Physics Research Section A: Accelerators, Spectrometers, Detectors and Associated Equipment* 987 (Jan. 2021), p. 164807. ISSN: 01689002. DOI: 10.1016/j.nima.2020.164807. URL: https://linkinghub.elsevier.com/retrieve/pii/S0168900220312043 (visited on 08/30/2024).

[15] M. Acciarri et al. “K0SK0S final state in two-photon collisions and implications for glueballs”. In: *Physics Letters B* 501.3 (Mar. 8, 2001), pp. 173–182. ISSN: 0370-2693. DOI: 10.1016/S0370-2693(01)00116-2. URL: https://www.sciencedirect.com/science/article/pii/S0370269301001162 (visited on 01/31/2025).

[16] Vincent Mathieu, Nikolai Kochelev, and Vicente Vento. “The physics of glueballs”. In: *International Journal of Modern Physics E* 18.1 (Jan. 2009). Publisher: World Scientific Publishing Co., pp. 1–49. ISSN: 0218-3013. DOI: 10.1142/S0218301309012124. URL: https://www.worldscientific.com/doi/abs/10.1142/S0218301309012124 (visited on 01/31/2025).

[17] The CLAS Collaboration et al. “Double ${K}_{S}^{0}$ photoproduction off the proton at CLAS”. In: *Physical Review C* 97.2 (Feb. 26, 2018). Publisher: American Physical Society, p. 025203. DOI: 10.1103/PhysRevC.97.025203. URL: https://link.aps.org/doi/10.1103/PhysRevC.97.025203 (visited on 01/30/2025).

[18] E. Crémieu-Alcan, Paul Falk-Vairant, and O. Lebey, eds. *Proceedings, Conférence Internationale d'Aix-en-Provence sur les Particules Elémentaires: Aix-en-Provence, France, Sep 14-20, 1961*. Gif-sur-Yvette, France: CEN, 1962.

[19] A. R. Erwin et al. "Experimental Cross Section for $\ensuremath{\pi}\ensuremath{\pi}\ensuremath{\rightarrow}K\overline{K}$". In: *Physical Review Letters* 9.1 (July 1, 1962). Publisher: American Physical Society, pp. 34–36. DOI: 10.1103/PhysRevLett.9.34. URL: https://link.aps.org/doi/10.1103/PhysRevLett.9.34 (visited on 01/31/2025).

[20] Gideon Alexander et al. "Final-State Interactions in the ${\ensuremath{\pi}}^{\ensuremath{-}}+p\ensuremath{\rightarrow}K+\overl Reaction". In: *Physical Review Letters* 9.11 (Dec. 1, 1962). Publisher: American Physical Society, pp. 460–464. DOI: 10.1103/PhysRevLett.9.460. URL: https://link.aps.org/doi/10.1103/PhysRevLett.9.460 (visited on 01/31/2025).

[21] David J. Crennell et al. "Observation of an Enhancement in the $I=0$ ${{K}_{1}}^{0}{{K}_{1}}^{0}$ System at 1068 MeV". In: *Physical Review Letters* 16.22 (May 30, 1966). Publisher: American Physical Society, pp. 1025–1029. DOI: 10.1103/PhysRevLett.16.1025. URL: https://link.aps.org/doi/10.1103/PhysRevLett.16.1025 (visited on 01/31/2025).

[22] Richard I. Hess et al. "Low-Mass $K\overline{K}$ Systems Produced in ${\ensuremath{\pi}}^{\ensuremath{-}}p$ Interactions Below 5 BeV/c". In: *Physical Review Letters* 17.21 (Nov. 21, 1966). Publisher: American Physical Society, pp. 1109–1112. DOI: 10.1103/PhysRevLett.17.1109. URL: https://link.aps.org/doi/10.1103/PhysRevLett.17.1109 (visited on 01/31/2025).

[23] Orin I. Dahl et al. "Strange-Particle Production in ${\ensuremath{\pi}}^{\ensuremath{-}}p$ Interactions from $1.5 \mathrm{to} 4.2 \frac{\mathrm{BeV}}{c}$. I. Three-and-More-Body Final States". In: *Physical Review* 163.5 (Nov. 25, 1967). Publisher: American Physical Society, pp. 1377–1429. DOI: 10.1103/PhysRev.163.1377. URL: https://link.aps.org/doi/10.1103/PhysRev.163.1377 (visited on 01/31/2025).

[24] W. Beusch et al. "Observation of resonance in the KO1KO1 system". In: *Physics Letters B* 25.5 (Sept. 18, 1967), pp. 357–361. ISSN: 0370-2693. DOI: 10.1016/0370-2693(67)90095-0. URL: https://www.sciencedirect.com/science/article/pii/0370269367900950 (visited on 01/31/2025).

[25] T. F. Hoang et al. "$K_{1}^{}{}_{}{}^{0}K_{1}^{}{}_{}{}^{0}$ Threshold Enhancement in ${\ensuremath{\pi}}^{\ensuremath{-}}p\ensuremath{\rightarrow}K_{1}^{}{}_{}{}^{0}K_{1}^{}{}_{}{}^{0}n$ at 4 and 5 GeV/c". In: *Physical Review Letters* 21.5 (July 29, 1968). Publisher: American Physical Society, pp. 316–319. DOI: 10.1103/PhysRevLett.21.316. URL: https://link.aps.org/doi/10.1103/PhysRevLett.21.316 (visited on 01/31/2025).

[26] T. F. Hoang et al. “Investigation of ${\ensuremath{\pi}}^{\ensuremath{-}}p\ensuremath{\rightarrow}K_{1}^{}{}_{}{}^{0}K_{1}^{}{}_{}{} at 4 and 5 GeV/c”. In: *Physical Review* 184.5 (Aug. 25, 1969). Publisher: American Physical Society, pp. 1363–1374. DOI: 10.1103/PhysRev.184.1363. URL: https://link.aps.org/doi/10.1103/PhysRev.184.1363 (visited on 01/31/2025).

[27] W. Beusch et al. “A new upper limit for the decay rate (f →)”. In: *Physics Letters B* 60.1 (Dec. 22, 1975), pp. 101–104. ISSN: 0370-2693. DOI: 10.1016/0370-2693(75)90539-0. URL: https://www.sciencedirect.com/science/article/pii/0370269375905390 (visited on 01/31/2025).

[28] W. Wetzel et al. “A study of → KK<math><mtext>K</mtext><mtext>K</mtext></math> using an experiment on p → KS0KS0n at 8.9 GeV/*c*”. In: *Nuclear Physics B* 115.2 (Nov. 22, 1976), pp. 208–236. ISSN: 0550-3213. DOI: 10.1016/0550-3213(76)90254-6. URL: https://www.sciencedirect.com/science/article/pii/0550321376902546 (visited on 01/31/2025).

[29] N. M. Cason et al. “Observation of a New Scalar Meson”. In: *Physical Review Letters* 36.25 (June 21, 1976). Publisher: American Physical Society, pp. 1485–1488. DOI: 10.1103/PhysRevLett.36.1485. URL: https://link.aps.org/doi/10.1103/PhysRevLett.36.1485 (visited on 01/30/2025).

[30] V. A. Polychronakos et al. “Study of the reaction ${\ensuremath{\pi}}^{\ensuremath{-}}p\ensuremath{\rightarrow}n{K}_{S}^{0}{K}_{ at 6.0 and 7.0 GeV/c”. In: *Physical Review D* 19.5 (Mar. 1, 1979). Publisher: American Physical Society, pp. 1317–1335. DOI: 10.1103/PhysRevD.19.1317. URL: https://link.aps.org/doi/10.1103/PhysRevD.19.1317 (visited on 01/31/2025).

[31] F. Barreiro et al. “Production and decay properties of f(1514) in Kp interactions at 4.2 GeV/*c*”. In: *Nuclear Physics B* 121.2 (Apr. 4, 1977), pp. 237–250. ISSN: 0550-3213. DOI: 10.1016/0550-3213(77)90436-9. URL: https://www.sciencedirect.com/science/article/pii/0550321377904369 (visited on 01/31/2025).

[32] S. R. Gottesman et al. “Peripheral production and decay of ${K}_{S}^{0}{K}_{S}^{0}$ in the reaction ${\ensuremath{\pi}}^{\ensurema }}p\ensuremath{\rightarrow}{K}_{S}^{0}{K}_{S}^{0}+\mathrm{neutrals}$ at 15.4 GeV/c”. In: *Physical Review D* 22.7 (Oct. 1, 1980). Publisher: American Physical Society, pp. 1503–1512. DOI: 10.1103/PhysRevD.22.1503. URL: https://link.aps.org/doi/10.1103/PhysRevD.22.1503 (visited on 01/30/2025).

[33] A. Etkin et al. “Amplitude analysis of the ${K}_{S}^{0}{K}_{S}^{0}$ system produced in the reaction ${\ensuremath{\pi}}^{\ensurema }}p\ensuremath{\rightarrow}{K}_{S}^{0}{K}_{S}^{0}n$ at 23 GeV/c”. In: *Physical Review D* 25.7 (Apr. 1, 1982). Publisher: American Physical Society, pp. 1786–1802. DOI: 10.1103/PhysRevD.25.1786. URL: https://link.aps.org/doi/10.1103/PhysRevD.25.1786 (visited on 01/31/2025).

[34] M. Althoff et al. "Production of KK-pairs<math><mtext>K</mtext><mtext>K</mtext><mtext>-pairs</mtext></math> in photon-photon collisions and the excitation of the tensor meson f(1515)". In: *Physics Letters B* 121.2 (Jan. 27, 1983), pp. 216–222. ISSN: 0370-2693. DOI: 10.1016/0370-2693(83)90917-6. URL: https://www.sciencedirect.com/science/article/pii/0370269383909176 (visited on 01/30/2025).

[35] R. S. Longacre et al. "A measurement of p→K0sK0sn at 22 GeV/c and a systematic study of the 2++ meson spectrum". In: *Physics Letters B* 177.2 (Sept. 11, 1986), pp. 223–227. ISSN: 0370-2693. DOI: 10.1016/0370-2693(86)91061-0. URL: https://www.sciencedirect.com/science/article/pii/0370269386910610 (visited on 01/31/2025).

[36] Christoph Berger et al. "Tensor Meson Excitation in the Reaction \gamma \gamma \to K^0_S K^0_S". In: *Z. Phys. C* 37 (1988), p. 329. DOI: 10.1007/BF01578125.

[37] D. Aston et al. "A study of the Ks0Ks0 system in the reaction Kp→Ks0Ks0 at 11 GeV/c". In: *Nuclear Physics B* 301.4 (May 16, 1988), pp. 525–553. ISSN: 0550-3213. DOI: 10.1016/0550-3213(88)90276-3. URL: https://www.sciencedirect.com/science/article/pii/0550321388902763 (visited on 01/31/2025).

[38] H. -J. Behrend et al. "TheKS0KS0final state in interactions". In: *Zeitschrift für Physik C Particles and Fields* 43.1 (Mar. 1, 1989), pp. 91–96. ISSN: 1431-5858. DOI: 10.1007/BF02430613. URL: https://doi.org/10.1007/BF02430613 (visited on 01/31/2025).

[39] M. Acciarri et al. "Study of the KS0KS0 final state in two-photon collisions". In: *Physics Letters B* 363.1 (Nov. 16, 1995), pp. 118–126. ISSN: 0370-2693. DOI: 10.1016/0370-2693(95)01041-N. URL: https://www.sciencedirect.com/science/article/pii/037026939501041N (visited on 01/31/2025).

[40] M. A. Reyes et al. "Partial Wave Analysis of the Centrally Produced ${K}_{S}{K}_{S}$ System at $800\phantom{\rule{0ex}{0ex}}GeV/\mathit{c}$". In: *Physical Review Letters* 81.19 (Nov. 9, 1998). Publisher: American Physical Society, pp. 4079–4082. DOI: 10.1103/PhysRevLett.81.4079. URL: https://link.aps.org/doi/10.1103/PhysRevLett.81.4079 (visited on 01/31/2025).

[41] B. P. Barkov et al. "Discovery of a narrow resonance state of the system KSKSat mass 1520 MeV". In: *Journal of Experimental and Theoretical Physics Letters* 70.4 (Aug. 1, 1999), pp. 248–253. ISSN: 1090-6487. DOI: 10.1134/1.568160. URL: https://doi.org/10.1134/1.568160 (visited on 01/31/2025).

[42] G. D. Tikhomirov et al. "Resonances in the KSKSKLsystem produced in collisions of negative pions with a carbon target at a momentum of 40 GeV". In: *Physics of Atomic Nuclei* 66.5 (May 1, 2003), pp. 828–835. ISSN: 1562-692X. DOI: 10.1134/1.1576456. URL: https://doi.org/10.1134/1.1576456 (visited on 01/31/2025).

[43] V. A. Schegelsky et al. "The K0 SK0 S final state in two-photon collisions and SU(3) tensor nonets". In: *The European Physical Journal A - Hadrons and Nuclei* 27.2 (Feb. 1, 2006), pp. 207–212. ISSN: 1434-601X. DOI: 10.1140/epja/i2005-10264-2. URL: https://doi.org/10.1140/epja/i2005-10264-2 (visited on 01/31/2025).

[44] V. V. Vladimirsky et al. "Analysis of the KSKS system from the reaction p → KSKSn at 40 GeV". In: *Physics of Atomic Nuclei* 69.3 (Mar. 1, 2006), pp. 493–509. ISSN: 1562-692X. DOI: 10.1134/S1063778806030124. URL: https://doi.org/10.1134/S1063778806030124 (visited on 01/30/2025).

[45] S. Uehara et al. "High-statistics study of K0S pair production in two-photon collisions". In: *Progress of Theoretical and Experimental Physics* 2013.12 (Dec. 1, 2013), p. 123C01. ISSN: 2050-3911. DOI: 10.1093/ptep/ptt097. URL: https://doi.org/10.1093/ptep/ptt097 (visited on 01/31/2025).

[46] M. Pivk and F.R. Le Diberder. "sPlot: A statistical tool to unfold data distributions". In: *Nuclear Instruments and Methods in Physics Research Section A: Accelerators, Spectrometers, Detectors and Associated Equipment* 555.1 (Dec. 2005), pp. 356–369. ISSN: 01689002. DOI: 10.1016/j.nima.2005.08.106. URL: https://linkinghub.elsevier.com/retrieve/pii/S0168900205018024 (visited on 08/30/2024).

[47] Hans Dembinski et al. "Custom Orthogonal Weight functions (COWs) for event classification". In: *Nuclear Instruments and Methods in Physics Research Section A: Accelerators, Spectrometers, Detectors and Associated Equipment* 1040 (Oct. 2022), p. 167270. ISSN: 01689002. DOI: 10.1016/j.nima.2022.167270. URL: https://linkinghub.elsevier.com/retrieve/pii/S0168900222006076 (visited on 08/30/2024).

[48] Hirotogu Akaike. "Information Theory and an Extension of the Maximum Likelihood Principle". In: *Selected Papers of Hirotugu Akaike*. Ed. by Emanuel Parzen, Kunio Tanabe, and Genshiro Kitagawa. New York, NY: Springer, 1998, pp. 199–213. ISBN: 978-1-4612-1694-0. DOI: 10.1007/978-1-4612-1694-0_15. URL: https://doi.org/10.1007/978-1-4612-1694-0_15 (visited on 02/01/2025).

[49] Gideon Schwarz. "Estimating the Dimension of a Model". In: *The Annals of Statistics* 6.2 (Mar. 1978). Publisher: Institute of Mathematical Statistics, pp. 461–464. ISSN: 0090-5364, 2168-8966. DOI: 10.1214/aos/1176344136. URL: https://projecteuclid.org/journals/annals-of-statistics/volume-6/issue-2/Estimating-the-Dimension-of-a-Model/10.1214/aos/1176344136.full (visited on 02/01/2025).